http://dx.doi.org/10.5012/bkcs.2013.34.5.1445

Synthesis and Characterization of $Zn_{(1-x)}Ni_xAl_2O_4$ Spinels as a New Heterogeneous Catalyst of Biginelli's Reaction

Fatima-Zohra Akika,[†] Nadjib Kihal,[†,¶] Tahir Habila,[†,¶] Ivalina Avramova,[‡] Şefik Suzer,[§] Bernard Pirotte,[#] and Smail Khelili[†,¶,*]

[†]*Département de Chimie, Faculté des Sciences Exactes et Informatique, Université de Jijel, BP. 98, Ouled Aissa 18034 Jijel, Algérie. [*]E-mail: skhelili@yahoo.fr*
[‡]*Institute of General and Inorganic Chemistry, Bulgarian Academy of Sciences, Acad G. Bonchev Blv., Block 11*
[§]*Department of Chemistry, Bilkent University, Main campus 068000 Ankara, Turkey*
[#]*Laboratoire de chimie pharmaceutique, CHU Tour 4, B36, Université de liège, 4000 Liège, Belgique*
[¶]*Equipe de Chimie Pharmaceutique, Laboratoire de Pharmacologie et de Phytochimie, Université de Jijel, BP. 98, Ouled Aissa 18034 Jijel, Algérie*
Received November 30, 2012, Accepted February 14, 2013

$Zn_{(1-x)}Ni_xAl_2O_4$ (x = 0.0-1.0) spinels were prepared at 800 °C by co-precipitation method and characterized by infrared spectroscopy, X-ray diffraction, scanning electron microscopy and X-ray photoelectron spectroscopy. The specific surface area was determined by BET. SEM image showed nano sized spherical particles. XPS confirmed the valence states of the metals, showing moderate Lewis character for the surface of materials. The powders were successfully used as new heterogeneous catalysts of Biginelli's reaction, a one-pot three-component reaction, leading to some dihydropyrimidinones (DHPMs). These new catalysts that produced good yields of DHPMs, were easily recovered by simple filtration and subsequently reused with persistent activity, and they are non-toxic and environmentally friendly. The optimum amount of catalyst is 20% by weight of benzaldehyde derivatives, while the doping amount has been found optimal for x = 0.1.

Key Words : Spinel, XRD, XPS, Catalytic properties, Biginelli's reaction

Introduction

Spinels are ternary oxides with the general formula AB_2O_4, where A and B are cations occupying tetrahedral and octahedral sites respectively.[1] The lattice belongs to the space group Fd3m (number 227 in the international table).[2,3] This distribution of cations is not always the most thermodynamically stable, since A and B cations may exchange interstices *via* diffusion, eventually leading to inverted spinel, where all the A cations occupy the octahedral interstices.[4]

Mixed oxides have interesting properties: they are widely used as ceramic pigments, magnetic devices, refractory materials and sensors, and in particular, as catalytic material (or catalyst support).[5-9] they also present optical and dielectric properties. For example, zinc aluminate $ZnAl_2O_4$ efficiently catalyses many chemical reactions, such as dehydration, hydrogenation and is used in the synthesis of fine chemicals.[10-12] Oxides spinels are usually synthesized by solid state reaction at high temperature,[14,15] sol gel, coprecipitation and hydrothermal methods are also used to prepare spinels at low temperature.[16-19] The coprecipitation method is reproducible, permits good stoichiometric control, and produces pure nano sized powders with high surface area. For these reasons, it becomes the most attractive technic. However, solid state method suffers from the lack of homogeneity of particles, the difficulty of stoichiometry control, implies high temperature, and produces materials with low surface area.

The Biginelli's reaction is a one pot condensation of an aldehyde, a β-keto ester and urea (or thiourea) under strong acid conditions, producing dihydropyrimidinones (DHPMs).[20] Recently, DHPMs received great interest because of their potential antiviral, antimitotic, anticarcinogenic, and antihypertensive (calcium channel modulators) properties.[21-25] However, this reaction suffers from low yields, relatively long reaction times, and some procedures require harmful and toxic solvents.[26] For these reasons, several attempts were undertaken to find alternative environmentally friendly synthesis routes. Indeed, some approaches have been developed using solvent free conditions, but the most attractive was the one which used microwave radiations and heterogeneous catalysts.[27,28] A wide variety of catalysts have been reported for Biginelli's reaction, in particular Lewis acids catalysis, such as $NiCl_2{\cdot}6H_2O$, $FeCl_3{\cdot}6H_2O$, In(III)-halides, $ZrCl_4$, lanthanide halides such as $LaCl_3{\cdot}7H_2O$, and $CeCl_3{\cdot}7H_2O$, but they were not reusable and recoverable after the end of the reaction.[29-33] Other expensive catalysts such as polystyrene-poly(ethylene glycol) (PS-PEG), covalently anchored sulfonic acid onto silica, and Al_2O_3/CH_3SO_3H, implying relatively long reaction times, were also used.[34-36] Metal triflates, such as $Zn(OTf)_2$, $Bi(OTf)_3$, or lanthanide triflates as $Yb(OTf)_3$, nano crystalline copper (II) oxide, and alumina supported MoO_3, were also reported, but, to our knowledge, no investigation on mixed oxides like spinels has been reported as catalysts of Biginelli's reaction.[37-41]

This paper reports the synthesis of mixed oxides $Zn_{(1-x)}$-

$Ni_xAl_2O_4$ (x = 0.0-1.0) type spinel, prepared by the co-precipitation method. The cristallinity and morphology were studied by X-ray diffraction (XRD), Fourier transform infrared spectra (FTIR), and scanning electron microscopy (SEM). The specific surface area was measured by BET technic and the surface state was investigated by X-ray photoelectron spectroscopy (XPS). The prepared powders were successfully used as catalysts of multicomponent Biginelli's reaction. We will present the effect of nickel (doping agent) content and the proportion of catalyst relative to benzaldehyde, on yields and time reaction, in relation to the surface structure and the catalyst composition. This work offers a new recoverable cheap heterogeneous catalyst, giving DHPMs with good yields, and relatively short time reaction. The catalyst was reusable up to five cycles and did not imply the use of toxic solvents.

Experimental

Catalyst Preparation. Zinc nitrate (1.4 g, Biochem 98%), nickel nitrate (0.15 g, Panreac 98.12%) and aluminium nitrate (3.8 g, Biochem 98%) were dissolved in distilled water and magnetically stirred for 15 minutes. The obtained solution was diluted and stirred again for 15 minutes. Then, a solution of 24% ammonia was slowly added until the solution became neutral and a chelate was formed. The resulting precipitate was filtered and heated in air, at 110 °C for 24 h. The obtained powders were ground and calcined at 400 °C for 8 h, in order to remove the nitrates, then at 600 °C and 800 °C, respectively, for 5 h until the formation of green fine powders.

Catalyst Characterization. The X-ray diffraction characterization was carried out at room temperature, with the Cu K_α monochromatic radiation ($\lambda = 1.54056$ Å) of a D8 Advance Bruker AXS diffractometer, operating at the accelerating voltage of 40 kV and filament current of 40 mA. Data were collected between 10° and 90° at 0.04°/step for a counting time of 5s. Data were analyzed using JCPDS standards and the resulting patterns were indexed by comparison with standard XRD patterns. Infrared spectra of samples, shaped as KBr pellets, were recorded in the range 400-4000 cm^{-1}, using a SHIMADZU 8400 spectrometer. Morphology and grain size of the powders were observed by ZEISS EVO40 scanning electron microscope (SEM) model, using an acceleration voltage of 20 KV. The surface area measurement of the powders was performed using a Tristar 300 equipment, after outgassing all the powders at 350 °C for 2 hours, using N_2 as the adsorption/desorption gas at 77 K. XPS measurements were performed on a Kratos 300 spectrometer equipped with a monochromatic Mg Kα source (1253.6 eV). The samples were out gassed under vacuum at 10^{-8} torr for several hours (12 h) before the analysis. All the spectra were calibrated in binding energy with reference to the C 1s peak of contamination fixed at 284.6 eV.[42] The photoemission peaks were fitted with mixed Gaussian-Lorentzian functions using a home-developed least squares curve-fitting program (Winspec). Shirley background subtraction were used for all the spectra.[43] The surface atomic composition was calculated by the integration of the peak areas on the basis of the scofield's sensitivity factors.[44] We also chose the C1s peak of contamination as internal reference to calculate the atomic composition (in at %) according to Eq. (1).

$$\frac{[X]}{[C]} = \frac{N_X \sigma_C \lambda_C}{N_C \sigma_X \lambda_X} \quad (1)$$

Where N is the experimentally determined peak intensity of X and carbon C subshell atoms affected by the photoionization, σ is the sensitive factor and λ is the mean free path of photoelectron in the sample.

As suggested for inorganic solids and binding energies below 1100 eV, we took $\lambda \sim Ec^{0.75}$ where E_c is the kinetic energy of electron ejected from the k^{th} shell of an atom atthe surface.

The ^1H NMR spectra of DHPMs were taken on a Bruker (500 MHz) instrument in DMSO-d_6, using hexamethyldisiloxane (HMDS) as an internal standard. Chemical shifts are reported in δ values (ppm) relative to internal HMDS. The abbreviations s = singlet, d = doublet, t = triplet, q = quadruplet, m = multiplet, and b = broad, were used throughout. Elemental analysis (C, H, N, S) were performed on a Carlo-Erba EA 1108-elemental analyser and were within 0.4% of theoretical values. All reactions were routinely checked by TLC on silica gel (Merck 60F 254).The melting points were recorded on a banc Kofler, and are uncorrected.

General Procedure for the Synthesis of 3,4-Dihydropyrimidin-2(1*H*)-ones/thiones. In a 50 mL flask, the mixture of aldehyde (5 mmol), ethyl acetoacetate (5 mmol), urea/thiourea (10 mmol) and Zn91 (20% w/aldehyde) in ethanol (10 mL) was stirred and refluxed for an appropriate time. After the end of reaction, the product was isolated by evaporating the solvent. Recrystallization from ethanol yields pure dihydropyrimidinones (thiones). The recovered catalyst was dried in an oven at 200 °C for 24 hours, and reused in subsequent reactions.

5-Ethoxycarbonyl-6-methyl-4-phenyl-3,4-dihydropyrimidin-2-(1*H*)-one (4a). Yield: 90%; mp 206-208 °C; IR (KBr) ν 3240, 3120, 1750, 1670, 1650, 1430-1430, 1200, 770; ^1H RMN (500 MHz, DMSO-d_6) δ 9.18 (br s, 1H, NH), 7.72 (br s, 1H, NH), 7.32-7.29 (m, 5H, arom CH), 5.16 (d, 1H, CH), 3.98 (q, 2H, CH_2), 2.25 (s, 3H, CH_3), 1.08 (t, 3H, CH_3). Anal. Calcd for $C_{14}H_{16}N_2O_3$: C, 64.60; H, 6.20; N, 10.76. Found: C, 64.58; H, 6.19; N, 10.77.

5-Ethoxycarbonyl-6-methyl-4-phenyl-3,4-dihydropyrimidin-2-(1*H*)-thione (4b). Yield: 62%; mp 204-206 °C; IR (KBr) ν 3320, 3130, 1670, 1575 1530-1440, 1290, 770; ^1H RMN (500 MHz, DMSO-d_6) δ 10.32 (s, 1H, NH), 9.64 (s, 1H, NH), 7.36-7.21 (m, 5H, arom CH), 5.18 (d, 1H, CH), 4.01 (q, 2H, CH_2), 2.29 (s, 3H, CH_3), 1.1 (t, 3H, CH_3). Anal. Calcd for $C_{14}H_{16}N_2O_2S$: C, 60.85; H, 5.84; N, 10.14; S, 11.60. Found: C, 60.86; H, 5.85; N, 10.13; S, 11.61.

5-Ethoxycarbonyl-6-methyl-4-(4-nitrophenyl)-3,4-dihydropyrimidin-2-(1*H*)-one (4c). Yield: 74%; mp 218-220

°C; IR (KBr) ν 3240, 3120, 1710, 1690, 1650, 1590, 1480, 1510, 1350, 1220, 790; ^{1}H RMN (500 MHz, DMSO-d_6) δ 9.35 (s, 1H, NH), 8.22 (d, 2H, arom CH), 7.88 (s, 1H, NH), 7.50 (d, 2H, arom CH), 5.27 (d, 1H, CH), 3.99 (q, 2H, CH_2), 2.27 (s, 3H, CH_3), 1.10 (t, 3H, CH_3). Anal. Calcd for $C_{14}H_{15}N_3O_5$: C, 55.08; H, 4.95; N, 13.76. Found: C, 55.07; H, 4.96; N, 13.75.

5-Ethoxycarbonyl-6-methyl-4-(3-nitrophenyl)-3,4-dihydropyrimidin-2-(1*H*)-one (4d). Yield: 82%; mp 226-228 °C; IR (KBr) ν 3320, 3120, 1720, 1640, 1530-1350, 1480, 1230, 780, 730; ^{1}H RMN (500 MHz, DMSO-d_6) δ 9.36 (s, 1H, NH), 8.15-8.13 (m, 1H, arom CH), 8.08 (s, 1H, arom CH), 7.89 (s, 1H, NH), 7.71-7.64 (m, 2H, arom CH), 5.30 (d, 1H, CH), 4.00 (q, 2H, $\underline{CH_2}CH_3$), 2.26 (s, 3H, CH_3), 1.01 (t, 3H, CH_3). Anal. Calcd for $C_{14}H_{15}N_3O_5$: C, 55.08; H, 4.95; N, 13.76. Found: C, 55.09; H, 4.94; N, 13.77.

5-Ethoxycarbonyl-6-methyl-4-(2-nitrophenyl)-3,4-dihydropyrimidin-2-(1*H*)-one (4e). Yield: 75%; mp 234-236 °C; IR (KBr) ν 3300, 3250, 1675, 1605, 1510, 1350, 1220, 780; ^{1}H RMN (500 MHz, DMSO-d_6) δ 10.10 (s, 1H, NH), 9.64 (s, 1H, NH), 8.16 (d, 1H, arom CH), 7.74 (d, 1H, CH), 7.80-7.25 (m, 3H, arom CH), 4.18 (q, 2H, CH_2), 2.21 (s, 3H, CH_3), 1.26 (t, 3H, CH_3). Anal. Calcd for $C_{14}H_{15}N_3O_5$: C, 55.08; H, 4.95; N, 13.76. Found: C, 55.06; H, 4.97; N, 13.75.

4-(4-Bromophenyl)-5-ethoxycarbonyl-6-methyl-3,4-dihydropyrimidin-2-(1*H*)-one (4f). Yield: 84%; mp 224-226 °C; IR (KBr) ν 3240, 3120, 1710, 1650, 1560, 1480, 1230, 790, 610; ^{1}H RMN (500 MHz, DMSO-d_6) δ 9.23 (s, 1H, NH), 7.76 (s, 1H, NH), 7.53 (d, 2H, arom CH), 7.19 (d, 2H, arom CH), 5.12 (d, 1H, CH), 3.98 (q, 2H, CH_2), 2.24 (s, 3H, CH_3), 1.01 (t, 3H, CH_3). Anal. Calcd for $C_{14}H_{15}BrN_2O_3$: C, 49.57; H, 4.46; N, 8.26. Found: C, 49.55; H, 4.45; N, 8.24.

4-(3-Bromophenyl)-5-ethoxycarbonyl-6-methyl-3,4-dihydropyrimidin-2-(1*H*)-one (4g). Yield: 66%; mp 198-200 °C; IR (KBr) ν 3200, 3120, 1720, 1650, 1600, 1490, 1220, 790, 690; ^{1}H RMN (500 MHz, DMSO-d_6) δ 9.26 (s, 1H, NH), 7.78 (s, 1H, NH), 7.46-7.23 (m, 4H, arom CH), 5.14 (d, 1H, CH), 3.99 (q, 2H, CH_2CH_3), 2.25 (s, 3H, CH_3), 1.10 (t, 3H, CH_3). Anal. Calcd for $C_{14}H_{15}BrN_2O_3$: C, 49.57; H, 4.46; N, 8.26. Found: C, 49.56; H, 4.44; N, 8.25.

5-Ethoxycarbonyl-4-(2-methoxy-5-bromophenyl)-6-methyl-3,4-dihydropyrimidin-2-(1*H*)-one (4h). Yield: 52%; mp 224-226 °C; IR (KBr) ν 3240, 3075, 1710, 1650, 1600, 1480, 1230, 750; ^{1}H RMN (500 MHz, DMSO-d_6) δ 9.18 (s, 1H, NH), 7.40 (m, 2H, NH + arom CH), 7.11 (s, 1H, arom CH), 6.97 (d, 1H, arom CH), 5.42 (d, 1H, CH), 3.93 (q, 2H, CH_2), 3.78 (s, 3H, CH_3), 2.27 (s, 3H, CH_3), 1,04 (t, 3H, CH_3). Anal. Calcd for $C_{15}H_{17}BrN_2O_4$: C, 48.80; H, 4.64; N, 7.59. Found: C, 48.79; H, 4.65; N, 7.60.

Results and Discussion

XRD Characterization. Figure 1(a) shows the powder X-ray diffraction patterns of $Zn_{(1-x)}Ni_xAl_2O_4$ (x = 0.0-1.0) obtained by calcination at 800 °C. The samples were essentially pure and revealed a single phase spinel type, except for x = 1 for which a secondary phase was observed.

The diffraction peaks of all samples are in accordance with the standard JCPDF card of $ZnAl_2O_4$.[45-47] They can be indexed as (220), (311), (400), (331), (422), (511), (440), (620) and (533) diffraction lines. Nevertheless, the peaks appearing at 2θ = 43.18°, 62.85°, 75.17°, and 79.14°, indexed as (200), (220), (311), and (222) diffraction lines, can be easily attributed to the face-centred cubic (FCC) crystalline structure of NiO (JCPDS, No. 04-0835). We note that the peak (111) was not observed because it was too weak and was covered by the most intense peak of spinel $NiAl_2O_4$.

In other hand, the powder X-ray patterns of the precursor (x = 0.1), annealed at different temperatures (400 °C, 600 °C, and 800 °C) for 5 h (Figure 1(b)) showed that the spinel structure begun to appear at relatively low temperature (400 °C). Then, the diffraction peaks progressively increased, particularly at 800 °C, indicating that the monophasic cubic spinel (Fd3m) became well crystalline.

Cell parameters were calculated by cell parameters refinement program (CELREF V3) in the 2θ range of 10-90°, and they are reported in Table 1. In general, the lattice para-

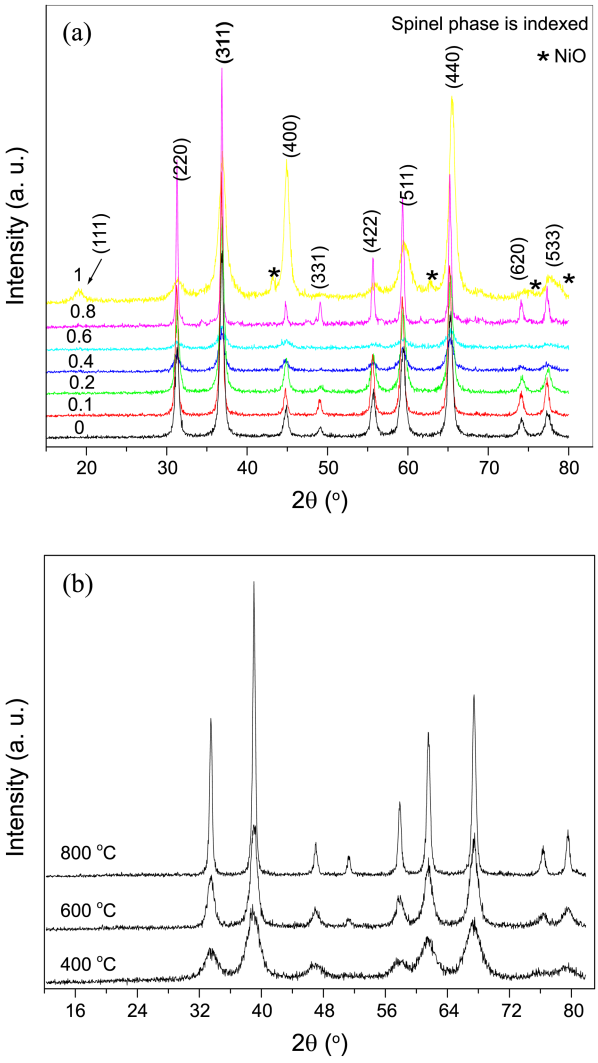

Figure 1. (a) Powder XRD patterns of $Zn_{(1-x)}Ni_xAl_2O_4$ oxides (x = 0.0-1.0) annealed at 800 °C. (b) Powder XRD patterns of $Zn_{(1-x)}Ni_xAl_2O_4$ (x = 0.1) heated at different temperatures.

Table 1. Lattice parameter a (Å) and average crystallite size of $Zn_{(1-x)}Ni_xAl_2O_4$ powders (x = 0.0-1.0)

x	a (Å)	d_{XRD} (nm)
0.0	8.0815	11.65
0.1	8.0784	17.85
0.2	8.0783	17.38
0.4	8.0788	12.70
0.6	8.0756	9.23
0.8	8.0684	9.07
1.0	8.0629	8.86

meters decrease with increasing of the nickel content. This variation can be attributed to the relatively smaller ionic radius of nickel with respect to zinc (0.74 and 0.69 Å respectively).[48]

The crystallite size d_{XRD} was calculated using Sherrer's equation from the XRD lines broadening using Eq. (2).[49]

$$d = \frac{K\lambda}{\beta\cos\theta} \quad (2)$$

Where β is the full-width at half-maximum (FWHM), K is the Scherrer crystal shape factor, generally close to unity (~0.9), λ is the wavelength of the X-ray source and θ is the Bragg's angle. The most intense peak (311) was used to calculate the crystallite size (d_{XRD}) and the results are reported in Table 1.

Infrared Spectroscopy (FTIR). Figure 2 reports the IR spectra of $Zn_{(1-x)}Ni_xAl_2O_4$ (x = 0.0-1.0). Some bands are common to the different contents of Ni. The band centered at about 3400 cm^{-1} can be attributed to the O-H longitudinal vibration of water, and the bands around 1650 cm^{-1} to the bending vibration of H-O-H. These bands are still present at high temperature; indicating that the adsorption phenomenon is very important on these types of oxides, which is probably related to the high surface areas of the material. The bands observed below 800 cm^{-1} can be assigned to the metal-oxide groups.[50] The most important bands are around 690 cm^{-1} and 545 cm^{-1}, can be related to bonds of the internal tetrahedral and octahedral sites of the spinel structure. The broadening of these bands can be assigned to the presence of more than one type of cation in the site.

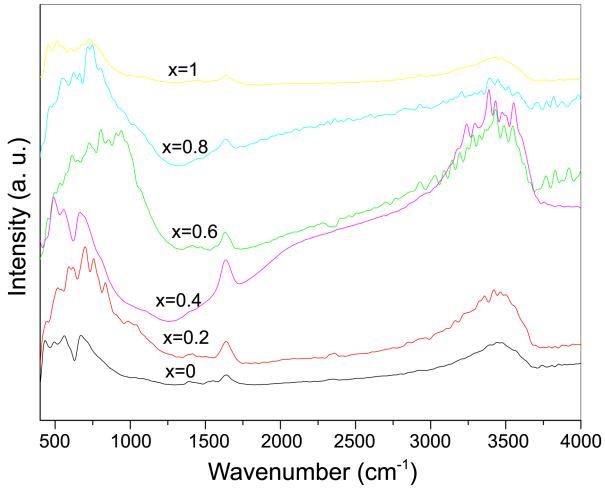

Figure 2. FTIR spectra of $Zn_{(1-x)}Ni_xAl_2O_4$ oxides (x = 0.0-1.0) prepared by co-precipitation method and annealed at 800 °C for 5 h.

Scanning Electron Microscopy (SEM). The SEM images (Figure 3(a) and 3(b)), for x = 0.2 and 0.8, respectively indicated that the morphology of the particles was homogenous and presented quasi-spherical grains with a nano metric scale. The nanoparticles sizes were estimated between 30 and 60 nm. These values were relatively different from those calculated from DRX (Table 1), mainly for the composition x = 0.8. This deviation proved that the particles are more agglomerated at the surface.

BET Measurement. The BET surface area (S_{BET}) and the most frequent pore volume (Vp) were estimated by the BET method.[51] The results are reported in Table 2. The S_{BET} values are very interesting, suggesting that this type of spinel could be used as catalysts in several reactions. On the one hand, S_{BET} firstly decreases (from x = 0 to 0.1), then increases (from x = 0.1 to 0.6), and decreases again for x = 0.8. Finally, they increases with a maximum value equal to 74.172 m^2/g for x = 1. On the other hand, V_p increases (from x = 0 to 0.2), then decreases (from x = 0.1 to x = 0.8) and finally increases for x = 1.

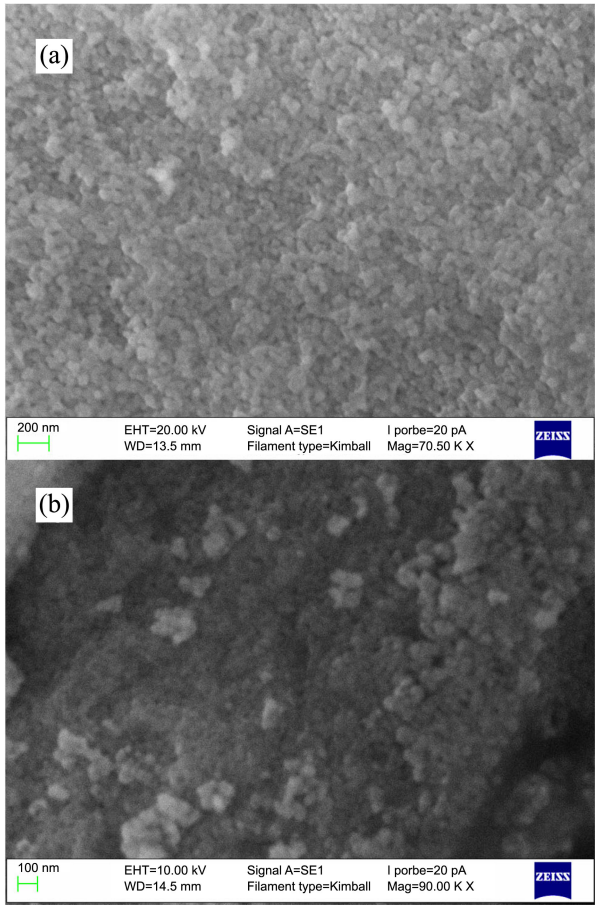

Figure 3. SEM images of the powders calcined at 800 °C: (a) x = 0.2. (b) x = 0.8.

Table 2. The results of the BET measurements: the surface area (S_{BET}), the pore volume (Vp) and the pore size (d_{BET}) (x = 0-1.0)

x	S_{BET} (m^2/g)	Vp (cm^3/g)	d_{BET} (nm)	S_{BET}/Vp
0.0	44.993	0.1170	28.90	384.56
0.1	24.824	0.188	52.92	132.04
0.2	44.403	0.197	29.47	225.40
0.4	42.917	0.103	30.72	416.70
0.6	65.371	0.0936	20.29	698.41
0.8	21.630	0.082	60.50	263.78
1.0	74.172	0.170	18.09	436.31

This irregular profile of variation of S_{BET} and Vp can be related to the powder agglomeration. Indeed, compared to the powders of submicron size, nanosized powders have a greater surface/volume ratio (Table 2). In order to minimize the total interfacial energy of the system, the particles are capable of forming Van Der Waals links between each other's. The Van der Waals attractions then cause the formation of agglomerates or aggregates. For this, most of the nano crystalline powders are not composed only of a nano scale particles (crystallites), formed by an individual crystal. But, the crystallites are connected together to form larger units known as agglomerates and aggregates.

The average diameter of crystallites (d_{BET}), assumed to be spherical (Table 2), was also calculated using Eq. (3):

$$d_{BET} = \frac{6}{A_s \rho} \quad (3)$$

Where A_S is the specific area (m^2/g) and ρ represents the theoretical density of the phase (g/cm^3). They are generally in agreement with the size observed by scanning electron microscopy (SEM). The average particle sizes found by chemisorption are systematically higher than the corresponding diameters estimated from XRD data.

XPS Analysis. The elemental composition of the surface of $Zn_{(1-x)}Ni_xAl_2O_4$ powders, annealed at 800 °C (x = 0.2, 0.8), can be observed from the survey XPS spectrum with a scan range from 0 to 1200 eV (Figure 4). All spectra were calibrated by reference to the C1s signal at 284.6 eV.

The percentages of the elements at the surface of samples (at %) for x = 0.2, 0.8 and the binding energies of their respective regions are summarized in Table 3.

It may be due, firstly, to the substitution of only a portion of zinc atoms by nickel, thus a deficiency in the structure can be envisaged; secondly, perhaps the nickel atoms are surrounded by high number of oxygen ions, so they can not easily migrate toward the surface. The XPS is normally used to investigate the state of the material surface, the nature of bonding (*e.g.* ionicity/covalency) and acid-base proprieties of oxides. So, it is reported hereafter the study of the most important peaks of the elements present at the surface (x = 0.2 and 0.8) mainly C1s, O1s, Zn2p and Al2p.

It is important to note that the carbon content is quite significant, particularly for x = 0.8. In general, carbon impurities have two origins: it may be introduced during the steps of sample preparation and by the adsorption of hydrocarbons inside the electron spectrometer.

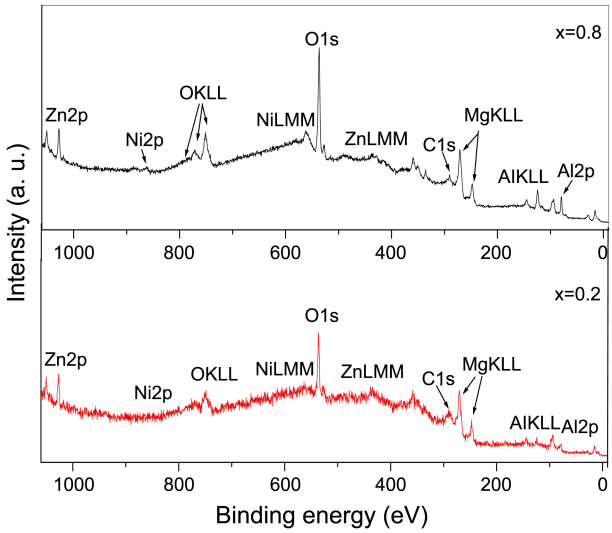

Figure 4. XPS survey spectrum of $Zn_{(1-x)}Ni_xAl_2O_4$ samples: x = 0.2 and 0.8.

Table 3. XPS analysis of the surface composition At (%) and binding energy (eV) for $Zn_{(1-x)}Ni_xAl_2O_4$ (with x = 0.2 and 0.8) samples

	Atomic composition (%)				
	Zn	Ni	Al	O	C
x = 0.2	4.85	1.18	21.90	55.34	16.72
x = 0.8	2.13	1.05	23.50	51.74	21.56
	Binding energy BE (eV)				
	Zn $2p_{3/2}$	Ni $2p_{3/2}$	Al2p	O1s	C1s
x = 0.2	1021.87	855.75	73.51	530.62	284.6
x = 0.8	2021.88	855.81	73.88	530.89	284.6
	[[Zn+] + [Al+] + [Ni+]]/[O][a]				
	x = 0.2	0.75			
	x = 0.8	0.69			

[a][O] represents the percentage of oxygen of the lattice; the contaminants O and C are not considered.

As an example, Figure 5(a) shows the C 1s core level spectra for the composition x = 0.2 and confirm this suggestion. Indeed, the spectra exhibits two features with different intensities: the most intense line at 284.61 eV is assigned to the carbon of natural contamination,[42] and the second larger one, located at 288.7 eV, is probably due to the CO_2 molecules adsorbed on the surface molecule.[52] It is very relevant to note the complete absence of the peak at ~286 eV, which characterizes the hydrocarbon organic molecules, and the peaks at ~282 eV, ~290 eV and 291.4 eV which excludes the formation of metal carbides and carbonate.

Figure 5(b) shows the curve fitting of Al 2p regions for the compositions x = 0.2 and 0.8 respectively.

The entire observed peaks can easily attributed to Al^{3+} linked to oxygen.[53,54] Those at 73.6 and 73.5 eV can be assigned to the bonds Al-O in oxides spinel,[55] the others,

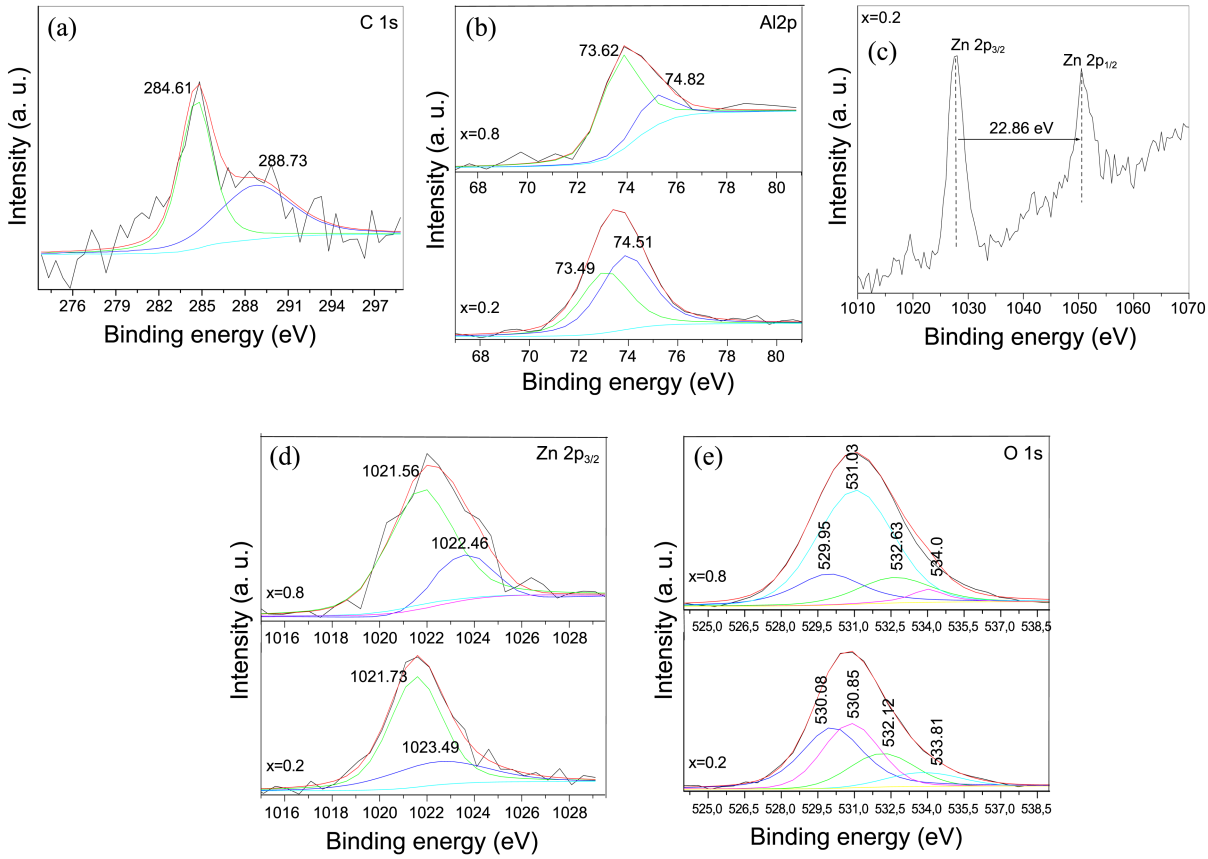

Figure 5. XPS regions of: (a) C 1s for x = 0.2; (b) Al 2p for x = 0.2, and 0.8; (c) Zn 2p for x = 0.2; (d) Zn 2p3/2 for x = 0.2 and 0.8; (e) O 1s for x = 0.2 and 0.8.

located at 74.5 and 74.8 eV, characterizes an hydroxide (OH) environment.[56]

The Zn 2p core level spectrum is characterized by two components appearing due to the spin-orbit splitting between Zn $2p_{3/2}$ and Zn $2p_{1/2}$. The observed value of the spin-orbit splitting for the composition x = 0.2 is 22.86 eV (Fig. 5(c)). Since the Zn $2p_{3/2}$ is the most intense, it can give more information on the chemical state of zinc. Indeed, the Zn $2p_{3/2}$ peaks of the respective samples are decomposed in two overlapping principal peaks (Figure 5(d)): the most intense (binding energies at 1021.56 eV for x = 0.8 and 1021.73 eV for x = 0.2) can be attributed to the chemical state of zinc as Zn^{2+}, and excluded practically the existence of zinc metal, while the peaks at higher energy (binding energies at 1023.49 eV for x = 0.2 and 1022.46 eV for x = 0.8) can be assigned to zinc hydroxides. These values are in agreement with those reported in the literature. Indeed, the binding energy of ZnO is located between 1021.6 and 1022.2 eV.[57]

In mixed oxides, the O 1s region is the most interesting to study, since the oxygen element binds with all the atoms in the material and can give more information. Therefore, the XPS spectra of O1s line related to the compositions x = 0.2 and 0.8 can be decomposed into four peaks (Fig. 5(e)). The two higher binding energies (at 532.12 and 533.81 eV for x = 0.2 and 532.61 and 534 eV for x = 0.8) are consistent with oxygen of organic compounds and adsorbed water respectively.[58,59] The other lower binding energies (530.08 and 530.85 eV for x = 0.2 and 529.95 and 531.03 eV for x = 0.8) can be undoubtedly attributed to the oxygen of the lattice.

According to Barr *et al.*,[60] Zn-O and Ni-O bonds have a normal ionic character and Al-O has a semi-covalent one. In the first case, it will be easier to eject the electron from the oxygen core level, so the XPS signal will be observed at lower energies and, in the second one, it will be more difficult to eject it. Therefore, the signal will be observed at higher energies. Consequently, energy values of 529.95 and 530.08 eV can be attributed to the Zn-O and Ni-O bonds and those at 530.85 and 531.08 eV can be assigned to the Al-O bonds.

Table 4 presents the percentages of components resulting from the deconvolution of O 1s peak (x = 0.2 and x = 0.8). We can see that the percentages of oxygen atoms involved in the crystal lattice of the two samples were 67.19% and 73.88% for x = 0.2 and x = 0.8 respectively. It is interesting to point out that the percentage of the component at 531.03 eV is very important (60.1%) for the sample x = 0.8. In our opinion it is due to the occupation of the octahedral sites by Ni^{2+} and Al^{3+} ions in the spinel structure. Indeed, the nickel aluminate spinel $NiAl_2O_4$ is almost inverted with the nickel ions preferentially distributed over the octahedral sites.[61]

In order to estimate the character of the materials surface, we have excluded all the contaminants, mainly CO_2 and H_2O. It is clear that the ratio of the sum of fractions of Al^{3+},

Table 4. Percentage of deconvoluted peaks of O 1s region for $Zn_{(1-x)}Ni_xAl_2O_4$ samples x = 0.2 and x = 0.8

Samples	BE (eV)	FWHM	Area (%)
0.2	530.08	2.4	33.29
	530.85	2.7	33.90
	532.12	1.2	21.11
	533.81	3.4	11.70
0.8	529.95	2.5	13.78
	531.03	2.3	60.10
	532.63	2.6	15.20
	543.00	3.3	10.92

Zn^{2+}, Ni^{2+} and that of the oxygen, for the two samples (x = 0.2 and 0.8), are 0.75 and 0.69 respectively (Table 3), which means that the surface possesses moderate character of a Lewis acid, and pronounced anionic character, which could predicts an interesting catalytic and electrochemical properties for these materials.

Catalytic Activity

The materials described above ($Zn_{(1-x)}Ni_xAl_2O_4$; x = 0.0-1.0), were used to catalyse Biginelli's reaction, to prepare dihydropyrimidinones **4** following the Scheme 1 given bellow. It is a multicomponent reaction, which implies the one pot condensation of an aromatic aldehyde **1**, urea or thiourea **2** and ethyl acetoacetate **3**. As revealed by XPS analysis, the surface of these materials is constituted by about one third of cations (Zn^{2+}, Ni^{2+} and Al^{3+}) which would make them good catalysts, due to the Lewis acid character and relatively high specific area.

First of all, the reaction was carried out using benzaldehyde, urea and ethyl acetoacetate, as reagents, in the presence of 10% catalyst, with varying x from 0 to 1. The aim is the determination of the value of x giving the optimal yields, associated to the shorter time of reaction.

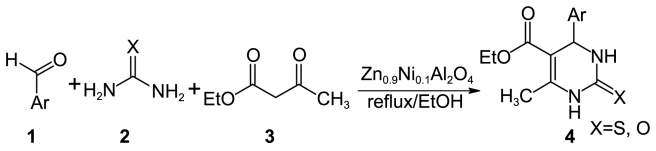

1 2 3 4

Scheme 1. Biginelli's reaction: starting materials, catalyst and final product.

Table 5. Synthesis [Yield (%) and time reaction] of DHPM using the $Zn_{(1-x)}Ni_xAl_2O_4$ catalysts

x in $Zn_{(1-x)}Ni_xAl_2O_4$	Yield (%)	Time (h)
0.0	42	10
0.1	90	4
0.2	83	4
0.4	80	5
0.6	54	6.5
0.8	23	12
1.0	62	6

Table 6. Amounts of catalyst ($Zn_{0.9}Ni_{0.1}Al_2O_4$), yields and reaction times

Amount of $Zn_{0.9}Ni_{0.1}Al_2O_4$ (%)	Yield (%)	Time (h)
5	30	6
10	76	4
20	90	4
25	90	4

As shown in Table 5, the best activity was obtained when $0.1 \leq x \leq 0.4$, and the most active catalyst ($Zn_{0.9}Ni_{0.1}Al_2O_4$) among the series was for x = 0.1, while the pore size was comprised between 29.47 and 52.92 nm. Yields are weaker for the other compositions of catalysts, which could be attributed to the particles agglomeration phenomena and the appearance of secondary phases for greater nickel contents of. The agglomeration of particles could limit the access of reagents to the catalytic sites.

Secondly, the reaction was carried out using the same reagents used above, but in presence of several amounts of the catalyst $Zn_{0.9}Ni_{0.1}Al_2O_4$, namely 5, 10, 20 and 25% (w/w Benzaldehyde). As shown in Table 6, the optimal amount of the catalyst was 20% w/w to benzaldehyde, corresponding to 90 of yield and four hours for reaction time.

Finally, the reaction was carried out using several benzaldehyde derivatives, urea or thiourea and ethyl acetoacetate, for which the results are presented in Table 7, and the

Table 7. Yields (%) of DHPMs up to five cycles and time reaction relative to $Zn_{0.9}Ni_{0.1}Al_2O_4$ catalyst

DHPMs	Ar	X	Time (h)	Yield (%)				
				Cycle 1	Cycle 2	Cycle 3	Cycle 4	Cycle 5
4a[62]	Ph	O	4	90	89	90	87	86
4b[63]	Ph	S	6	62	61	60	63	62
4c	4-NO_2-Ph	O	7	74	74	73	72	73
4d[64]	3-NO_2-Ph	O	6	82	82	81	82	80
4e[65]	2-NO_2-Ph	O	7	75	75	74	75	73
4f[66]	4-Br-Ph	O	6.5	84	84	82	83	80
4g	3-Br-Ph	O	7	66	65	64	66	63
4h	5-Br-2-OMe-Ph	O	8	52	50	51	49	50

structures of prepared DHPMs were confirmed by IR, ^{1}H NMR and elemental analysis, and presented above.

By examining the results, we note that, whatever the substituent of the aromatic ring of aldehyde yields were excellent. Thiourea is relatively less reactive than urea. The catalyst was reused five times without significant loss of its catalytic activity which is regenerated by simple heating at 200 °C. We can say that the catalyst, submitted to contact of organic chemicals used in the Biginelli's reaction, possesses a good chemical stability and persistent catalytic properties.

Conclusion

Polycrystalline nano sized zinc aluminates doped with nickel in the system $Zn_{(1-x)}Ni_xAl_2O_4$ (x = 0.0-1.0) were successfully synthesized by co-precipitation method using ammonia as a chelating agent. All the structures are pure and present single spinel phase after calcinations at 800 °C. The morphology of the particles was quasi-spherical with an average size of the grains about 30-60 nm. The IR spectrum revealed bands related to the inorganic network and characteristic to the spinel structure. The specific surface areas determined by BET surface area measurement were very significant and the surface analysis of this type of catalysts, carried out by X-ray photoelectron (XPS), shown that the surface possesses a moderate Lewis acid character. We have developed a new catalyst $Zn_{0.9}Ni_{0.1}Al_2O_4$ as a new and mild Lewis acid promoter in the multicomponent Biginelli's reaction. Besides its simplicity and mild reaction conditions, this method was effective with a variety of substituted aromatic aldehydes independently of the nature of the substituents in the aromatic ring, representing an improvement to the classical Biginelli's reaction. This new catalyst which has a good chemical stability and relatively persistent catalytic properties will be used to catalyse other multicomponent reactions.

Acknowledgments. We are thankful to Hikmet Sezen for assisting in the XPS measurements and to Eda Özkaraoglu for SEM images and EDAX analysis (Ankara, Turkey). (Ankara, Turkey). Our thanks also go to director and stuff of laboratory of phytochemistry and pharmacology (Jijel University) for logistic help. And the publication cost of this paper was supported by the Korean Chemical Society.

References

1. Bragg, W. H. The Structure of the Spinel Group of Crystals. *Phil. Math*. **1915**, *30*, 305.
2. Hahn, T. *International Tables for X-ray Crystallography*: *Space Group Symmetry*; 2006; vol. *A*. chap. 7.1, p 669.
3. Nishikawa, S. *Proc. Math. Phys. Soc*. Tokyo, Japan, **1915**, *8*, 199.
4. O'Neill, H. St. C.; Dollase, W. A. *Phys. Chem. Minerals* **1994**, *20*, 541.
5. Nathawan, P.; Darshane, V. S. *Structural J. Phys.* **1988**, *2*, 3191.
6. Van der Laag, N. J.; Snel, M. D.; Magusin, P. C. M. M.; De With, G. *J. Eur. Cer. Soc.* **2004**, *24*, 2417.
7. Chen, L.; Horiuchi, T.; Mori, T. *Appl. Catal. A. Gen*. **2001**, *209*, 97.
8. Shangguan, W. F.; Teraoka, Y.; Kagawa, S. *Appl. Catal. B: Environ.* **1996**, *8*, 217.
9. Seiyama, N.; Yamazoe N.; Arai, H. *Sensors and Actuators* **1983**, *4*, 85.
10. Shioyama, T. K.; Alcohol Dehydratation Employing Zinc Aluminate Catalysis, U.S. Patent Number 4, 260, 845, date of patent 1981.
11. Aguilar-Rios, G.; Valenzuela, M.; Salas, P.; Armendariz, M.; Bosh, P.; Del Toro, G.; Silva, R.; Bertin, V.; Castillo, S.; Ramirez-solis, A.; Schifter, I. *Appl. Catal. A. Gen.* **1995**, *127*, 65.
12. Roesky, R.; Weiguny, J.; Bestgen, H. B.; Dingerdissen, U. *Appl. Catal. A: General* **1999**, *176*, 213.
13. Muhammad Abdul Jamal, E.; Sakthi Kumar, D.; Antharaman, M. R. *Bull. Mater. Sci.* **2011**, *34*, 251.
14. Sampath, K.; Cordino, F. *J. Amer. Ceram. Soc.* **1998**, *81*, 649.
15. Hong, W. S.; De Jonghe, L. C. *J. Am. Ceram. Soc.* **1995**, *78*, 3217.
16. Phani, A. R.; Passacantando, M.; Santucci, S. *Mater. Chem. Phys*. **2001**, *68*, 66.
17. Hetting, G. F.; Worl, H.; Weiter, H. H. Z. *Anorg. Allg. Chem*. **1956**, *283*, 207.
18. Valenzuela, M. A.; Jacobs, J. P.; Bosch, P.; Reije, S.; Zapata, B.; Brongersman, H. H. *Appl. Catal. A: General* **1997**, *148*, 315.
19. Chen, Z.; Shi, E.; Zheng, Y.; Li, W.; Wu, N.; Zhong, W. *Mater. Lett*. **2002**, *56*, 601.
20. (a) Biginelli, P. *Ber. Dtsch. Chem. Ges.* **1891**, *24*, 2962. (b) Biginelli, P. *Gazz. Chim. Ital*. **1893**, *23*, 360.
21. Hurst, E. W.; Hull, R. *J. Med. Chem.* **1961**, *3*, 215.
22. Mayer, T. U.; Kapoor, T. M.; Haggarty, S. J.; King, R. W.; Schreiber, S. I.; Mitchison, T. J. *Science* **1999**, *286*, 971.
23. Kato, T. *Jpn. Kokay Tokkyo Koho* **1984**, *59*, 190,974 (CA 102: 132067).
24. (a) Atwal, K. S.; Swanson, B. N.; Unger, S. E.; Floyd, D. M.; Moreland, S.; Hedberg, A.; O'Reilly, B. C. *J. Med. Chem.* **1991**, *34*, 806. (b) Rovnyak, G. C.; Atwal, K. S.; Hedberg, A.; Kimball, S. D.; Moreland, S.; Gougoutas, J. Z.; O'Reilley, B. C.; Schwartz, J.; Malley, M. F. *J. Med. Chem.* **1992**, *35*, 3254.
25. (a) Kape, C. O. *Molecules* **1998**, *3*(1), 1. (b) Jauk, B.; Pernat, T.; Kappe, C. O. *Molecules* **2000**, *5*, 227.
26. Ranu, B. C.; Hajra, A.; Jana, U. *J. Org. Chem.* **2000**, *65*, 6270.
27. (a) Dondoni, A.; Massi, A. *Tetrahedron Lett.* **2001**, *42*, 7975. (b) Choudhary, V. R.; Tillu, V. H.; Narkhede, V. S.; Borate, H. B.; Wakhakar, R. D. *Catal. Commun.* **2003**, *4*, 449.
28. (a) Stadler, A.; Kappe, C. O. *J. Comb. Chem.* **2001**, *3*, 624. (b) Stadler, A.; Yousefi, B. H.; Dallinger, D.; Walla, P.; Van der Eycken, E.; Kaval, N.; Kappe, C. O. *Org. Process Res. Dev.* **2003**, *7*, 707.
29. (a) Lu, L.; Ma, M. *Synlett.* **2000**, *1*, 63. (b) Lu, L.; Bai, Y. *Synthesis* **2002**, *4*, 466.
30. (a) Ranu, B. C.; Hajra, A.; Jana, U. *J. Org. Chem.* **2000**, *65*, 6270. (b) Fu, N.-Y.; Yuan, Y.-F.; Cao, Z.; Wang, S. W.; Wang, J.-T.; Peppe, C. *Tetrahedron* **2002**, *58*, 4801. (c) Fu, N.-Y.; Yuan, Y.-F.; Pang, M.-L.; Wang, J.-T.; Peppe, C. *J. Oragnomet. Chem.* **2003**, *672*, 52.
31. Reddy, C. V.; Mahesh, M.; Raju, P. V. K.; Babu, T. R.; Reddy, V. V. N. *Tetrahedron Lett*. **2002**, *43*, 2657.
32. Lu, J.; Bay, Y.; Wang, Z.; Yang, B.; Ma, H. *Tetrahedron Lett.* **2000**, *41*, 9075.
33. Bose, D. S.; Fatima, L.; Mereyala, H. B. *J. Org. Chem.* **2003**, *68*, 587-590.
34. Quan, Z.-J.; Da, Y.-X.; Zhang, Z.; Wang, X.-C. *Catalysis Communication* **2009**, *10*, 1146.
35. Gupta, R.; Paul, S.; Gupta, R. *Journal of Molecular Catalysis A: Chemica.* **2007**, *266*, 50.
36. Sharghi, H.; Jokar, M. *Synthetic Communications* **2009**, *39*, 958.
37. Xu, H.; Wang, Y-G. *Chinese J. Chem.* **2003**, *21*, 327.
38. Varala, R.; Alam, M. M.; Adapa, S. R. *Synlett.* **2003**, 67.
39. Ma, Y.; Qian, C.; Wang, L.; Yuang, M. *J. Org. Chem.* **2000**, *65*, 3864.
40. Jain, S. L.; Prasad, V. V. D. N.; Sain, B. *Catalysis Communications* **2008**, *9*, 499.
41. Kantam, M. L.; Ramani, T.; Chakrapani, L.; Choudary, B. M. **2009**,

10, 370.
42. Barr, T. L.; Seal, S.; Bozniak, K.; Klinowski, J. *J. Chem. Soc. Faraday Trans.* **1997**, *93*(1), 181-186.
43. Shirley, D. A. *Physical Review B* **1972**, *5*, 4709.
44. Wagner, C. D., Ed.; Empirically derived atomic sensitivity factor for XPS In: *Practical Surface Analysis 1: Auger and X-Ray Spectroscopy*; Brings and M. P. Seach, Willey: Chichester 1990; p 635. Appendix 6.
45. Altermatt, U. D.; Brown, I. D. *Acta Cryst.* **1987**, *A43*, 125.
46. Zawadzki, M. *Sol. State Sci*. **2006**, *8*, 14.
47. JCPDS PDF No 05-0669.
48. Shanon, R. D. *Acta Cryst. A32* **1976**, 751.
49. Cullity, B. D. *Elements of X-Ray Diffraction*; Addison-Wesley: London, U.K., 1978; p 101.
50. (a) Sigel, G. A.; Bartlett, R. A.; Decker, D.; Olmstead, M. M.; Power, P. P. *Inorg. Chem.* **1987**, *26*, 1773. (b) Adams, R. W.; Martin, R. L.; Winter, G. *Aust. J. Chem*. **1970**, *20*, 773. (c) Barraclough, C. G.; Bradley, D. C.; Lewis, J.; Thomas, I. M. *J. Chem. Soc.* **1961**, 2601.
51. Ettre, L. S. Pigment Surface, In: Lewis, P. A., Ed.; *Pigment Handbook*; Wiley-Interscience Publication: Ohio, U.S.A., 1987; p 139.
52. Barr, T. L. *J. Vac. Sci. Technol. A* **1989**, *7*, 1677.
53. Fritsh, A.; Légaré, P. *Surf. Sci.* **1987**, *186*, 247.
54. Cocke, D. L.; Johnson, E. D.; Merrill, R. P. *Catal. Rev. Sci. Eng.* **1984**, *26*, 163.
55. Benoit, R. lasurface, www.Lasurface.com/XPS and AES database.
56. Van den Brand, J.; Snijders, P. C.; Sloof, W. G.; Terryn, H.; de Wit, J. H. W. *J. Phys. Chem. B* **2004**, *108*, 6017.
57. Velu, S.; Suzuki, K.; Vijayaraj, M.; Barmann, S.; Gopinath, C. S. *Appl. Catal.* **2005**, *B55*, 287.
58. Rousseau, S.; Loridant, S.; Delichere, P.; Boreave, A.; Deloume, J. P.; Vernaux, P. *Applied Catalysis B: Environmenta* **2009**, *88*, 438.
59. Vincent Crist, B.; XPS international, LLC; PDF Handbooks of Monochromatic XPS Spectra 2005.
60. Barr, T. L.; Seal, S.; He, H.; Klinowski, J. *Vacuum* **1995**, *46*, 1391.
61. Arean, C. O.; Mentrait, M. P.; Lopez, A. J. L.; Parra, J. B. *Colloids Surf. A: Physicochem. Engg. Aspects* **200**1, *180*, 253.
62. Salitha, G.; Reddy, G. S. K.; Yadav, J. S. *Tetrahedron Lett*. **2003**, *44*, 6497.
63. Amini, M. M.; Shaabani, A.; Bazgir, A. *Catal. Commun*. **2006**, *7*, 843.
64. Mitra, A. K.; Banerjee, K. *Synlett*. **2003**, *10*, 1509.
65. Hevari, M. M.; Bakhtiara, K.; Bamoharam, F. Z. *Catal. Commun*. **2006**, *7*, 373.
66. Russowsky, D.; Lopes, F. A.; Silva, V. S. S.; Canto, K. F. S.; Montes D'Oca, M. G.; Godoi, M. N. *J. Braz. Chem. Soc.* **2004**, *15*, 165.